Electrochemical and Solid-State Letters, **5** (7) A145-A148 (2002)
0013-4651/2002/5(7)/A145/4/$7.00 © The Electrochemical Society, Inc.

Charge, Potential, and Phase Stability of Layered $Li(Ni_{0.5}Mn_{0.5})O_2$

J. Reed and G. Ceder*,z

Department of Materials Science and Engineering, Massachusetts Institute of Technology, Cambridge, Massachusetts 02139, USA

$Li(Ni,Mn)O_2$ materials have recently shown promise as high capacity stable electrodes for advanced rechargeable lithium batteries. Using first principles quantum mechanical energy computations we demonstrate that the stability of these materials is due to the particular valence distribution on the transition metals in this material. Spin density calculations indicate that the Mn ion has oxidation state +4 independently of the Li content in the material, while Ni is oxidized from Ni^{2+} to Ni^{4+} upon removing Li. The high insertion voltage for the $LiNi_{0.5}Mn_{0.5}O_2$ can be partly attributed to the change in Mn-Ni interaction upon Li cycling.
 [DOI: 10.1149/1.1480135]

Manuscript submitted November 17, 2001; revised manuscript received March 7, 2002. Available electronically April 25, 2002.

Layered lithium-manganese oxides are of interest for use in rechargeable lithium batteries because of their potential for very high capacity, relative safety, and affordability. Their inherent safety is derived from the fact that both Mn^{3+} (present at the end of discharge) and Mn^{4+} (at the end of charge) are quite stable valence states. While manganese oxides with the spinel structure and stoichiometry $LiMn_2O_4$ have been used in batteries, their capacity is limited, and severe stability issues exist with the material. Layered lithium manganese oxides, on the other hand, have a theoretical capacity of 288 mAh/g. Unfortunately, the layered α-$NaFeO_2$ structure is not the ground state for $LiMnO_2$[1] and one has to resort to either metastable processing routes[2,3] starting from a $NaMnO_2$, or to compositional modifications to increase the stability of the layered phase over the other possible polytopes.[4-7] Almost all of the pure or lightly doped layered manganese oxides have shown a rapid transformation to a spinel upon cycling.[8,9] While this spinel can in some cases maintain capacity,[10] it has a less favorable voltage profile and the remaining disorder in the structure limits its current density.

Using higher doping levels, it has been possible to stabilize the layered structure against transformation to spinel. In particular, co-doping of Li and Cr[5,11] has been particularly successful. Ni-doped Mn materials were first synthesized several years ago,[12,13] but this approach has gained renewed interest now that good cycling behavior for these materials has been demonstrated.[5,14]

Some uncertainty exists with regards to the valence states in these mixed-metal compounds. In $Li(Li,Cr,Mn)O_2$ the observed capacity could only be explained by the cycling of Cr^{3+} to Cr^{6+},[5] a fact later confirmed with X-ray absorption spectroscopy.[15] In $LiNi_{0.5}Mn_{0.5}O_2$ it has been speculated[5,14] that the Ni and Mn ions, respectively, have valence +2 and +4, though earlier work by Spahr[13] assumed both Ni and Mn to have valence +3 in the starting material. Because the capacity of $LiNi_{0.5}Mn_{0.5}O_2$ is >200 mAh/g, the assumption of Ni^{2+} and Mn^{4+} in the starting material requires that the nickel ion cycles between Ni^{2+} and Ni^{4+}. The purpose of this paper is to clarify the valence states in $LiNi_{0.5}Mn_{0.5}O_2$ and characterize the electronic and structural changes that occur upon delithiation. The origin for the high potential of this material is also discussed. The energies, intercalation potentials, geometries, and electronic structure of the $Li_xNi_{0.5}Mn_{0.5}O_2$ materials are obtained using first principles quantum mechanical computations in the generalized gradient approximation to density functional theory. Ultrasoft pseudopotentials and the Perdew-Wang exchange correlation function were used, as implemented in VASP.[16] All calculations were performed with spin polarization, previously demonstrated to be crucial in manganese oxides.[1] Reasonable intercalation potentials and geometrical information can be obtained with first principles methods, as has been amply demonstrated.[17-19] To describe the $LiNi_{0.5}Mn_{0.5}O_2$ system, a supercell with two formula units was used. Because this computational approach requires the use of periodic cells (as do most computational methods), the Mn and Ni are long-range ordered in rows on the triangular lattice of transition metal sites. In all cells, the symmetry was lowered enough (lower than that associated with Li/vacancy or Ni/Mn ordering alone) so that Jahn-Teller distortions could take place if energetically favorable. In practice, this means that the symmetry is always a subgroup of the *C*2/*m* group of the monoclinic layered $LiMnO_2$.

The valence state of a high-spin transition metal ion can best be determined by integrating the spin-polarization density in a sphere around the ion. Integrating spin density is much more effective than integrating the charge density, as the former filters out the electronic contribution from the oxygen p-states which usually carry very little net electron spin. For the relevant ions, Mn^{4+}, Mn^{3+}, and Mn^{2+}, we expect a total electron spin count of, respectively, 3, 4, and 5 (in units of 1/2 μ_B). For Ni^{4+}, Ni^{3+}, and Ni^{2+} we expect 0, 1, and 2, respectively, electron spins as the Ni^{4+} has a core of nonspin polarized, full t_{2g} levels. Figure 1a shows the integrated spin as function of integration radius around Ni and Mn in the $LiNi_{0.5}Mn_{0.5}O_2$ structure. The integrated moment increases steeply as we integrate through the d-states of the metal ion, but then reaches a plateau value because the charge density of the oxygen ions does not contribute to the spin density. After this plateau the integrated value increases again as spin from neighboring transition metals is picked up. The Mn ion in $LiNi_{0.5}Mn_{0.5}O_2$ clearly carries three electrons, corresponding to a valence of Mn^{4+}. The moment around Ni is slightly below what is expected for Ni^{2+}. The remainder of the moment is probably on the oxygen ions as is typical for nickel oxides. Some evidence for this lies in the fact that the point where the integrated spin density rises from the plateau value is at a shorter radius than for the Mn^{4+} ion. The spin integration in Fig. 1a indicates that the formal valence states are $LiNi_{0.5}^{II}Mn_{0.5}^{IV}O_2$. Further evidence can be found from the changes in spin density upon lithium removal. Figure 1b shows similar spin integrations for the delithiated material $Ni_{0.5}Mn_{0.5}O_2$. The spin on Mn is barely different from what it is in the fully lithiated material, while Ni has lost most of its moment, consistent with the electron configuration for Ni^{4+} in $Ni_{0.5}Mn_{0.5}O_2$. Figure 1a and b offer strong evidence that in $LiNi_{0.5}Mn_{0.5}O_2$ the correct valence assignment is Ni^{2+} and Mn^{4+}. Upon Li removal Ni^{+2} is oxidized to Ni^{4+} while the Mn^{4+} ion remains unchanged.

The selective oxidation of Ni in these materials is also consistent with the metal-oxygen bond length variations predicted from the computations (Fig. 2). Ni-O and Mn-O are separately shown in $LiNi_{0.5}Mn_{0.5}O_2$, $Li_{0.5}Ni_{0.5}Mn_{0.5}O_2$, and $Ni_{0.5}Mn_{0.5}O_2$. The vertical bars on the result indicate the variation in bond length in the struc-

* Electrochemical Society Active Member.
z E-mail: gceder@mit.edu

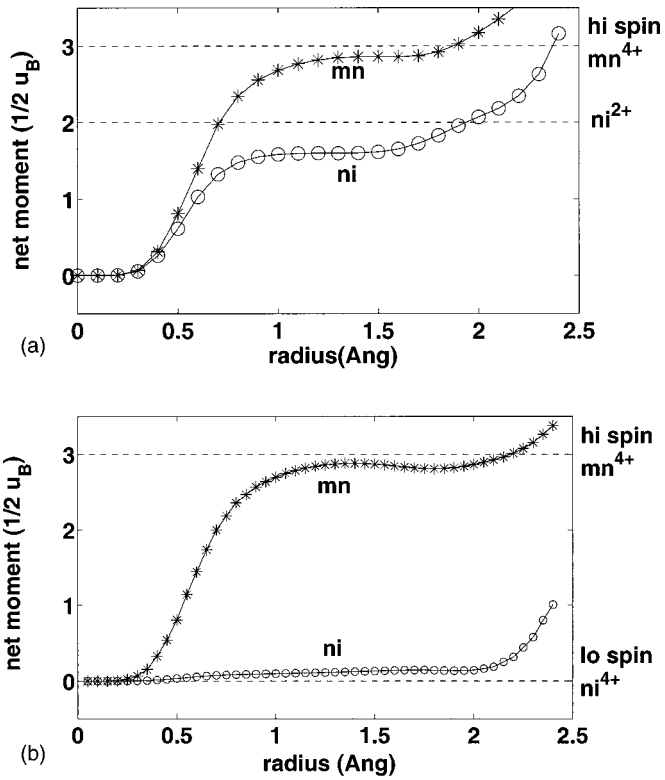

Figure 1. (a) Integrated spin as a function of integration radius (Å) around Ni and Mn in $LiNi_{1/2}Mn_{1/2}O_2$. (b) Integrated spin as a function of integration radius (Å) around Ni and Mn in $Ni_{1/2}Mn_{1/2}O_2$.

ture because the symmetry of our supercell (lower than $R\bar{3}m$) allows for slightly different bond lengths in a given octahedron. The Mn-O bond length hardly varies with Li composition, confirming that little or no change to its valence state occurs. In contrast, the Ni-O bond length changes dramatically with Li composition. For the delithiated material, the Ni-O bond length is around 1.90 Å, very typical of Ni^{4+}.[20,21] The very large spread in Ni-O distances at $x_{Li} = 0.5$ is due to the Jahn-Teller distortion around Ni^{3+} ion. The Jahn-Teller distortion is of the positive Q3 type,[22] so that there are four short and two long bonds. In a real material, the spread in bond lengths may be somewhat less due to the disorder of the Ni/Mn ions. Table I shows the calculated and experimentally measured lattice parameters. The calculated numbers are somewhat larger than those measured, as is often the case for computations in the generalized gradient approximation.

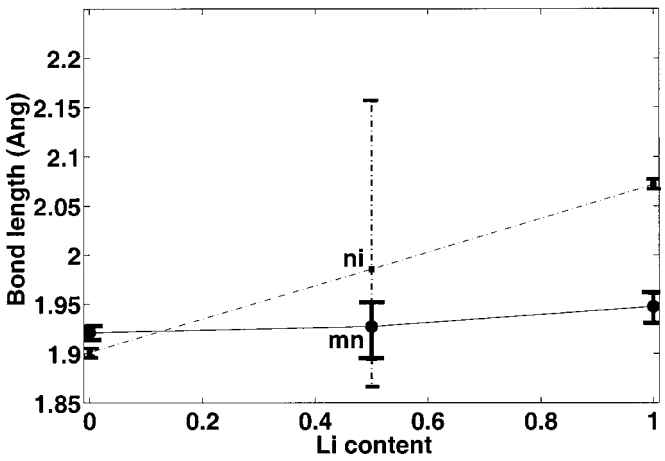

Figure 2. Plot of Ni-O (-··-) and Mn-O (——) bond lengths as a function of lithium content. Calculations performed at compositions of $LiNi_{1/2}Mn_{1/2}O_2$, $Li_{1/2}Ni_{1/2}Mn_{1/2}O_2$, and $Ni_{1/2}Mn_{1/2}O_2$. The data points correspond to the average bond lengths while the bars at each point indicate the spread between the maximum and minimum bond lengths. Note that at 1/2 lithium content the minimum Ni-O bond length is less than the minimum Mn-O bond length, while the maximum Ni-O bond length is greater than the maximum Mn-O bond length. This is due to the Ni^{3+} undergoing a Jahn-Teller distortion.

We have also calculated the average discharge potential for the system $LiNi_{0.5}Mn_{0.5}O_2/Ni_{0.5}Mn_{0.5}O_2$. These are compared to experimental data in Table II. The calculated potentials are below the experimental values, as is typical with standard first principles energy methods.[17] Hence, to make a better prediction possible, we have estimated a correction based on the difference between measured and calculated potentials for $LiNiO_2$. This correction (+0.73 V) is added to the calculated potential to give the result in the last column. We emphasize that this adjustment is purely phenomenological and for the purpose of facilitating the direct comparison with experiments for $LiNi_{0.5}Mn_{0.5}O_2$. The data in this column agrees well with the measured values for $LiNi_{0.5}Mn_{0.5}O_2$. In the last row of the table the potential is broken down into the average for the interval $LiNi_{0.5}Mn_{0.5}O_2$ to $Li_{0.5}Ni_{0.5}Mn_{0.5}O_2$, and $Li_{0.5}Ni_{0.5}Mn_{0.5}O_2$ to $Ni_{0.5}Mn_{0.5}O_2$. Some indication of the variation of potential upon charge can be derived from this.

Table II highlights the fact that the potential of $LiNi_{0.5}Mn_{0.5}O_2$ is actually very close to that of $LiNiO_2$. This is surprising because our results indicate that different redox couples are active in both materials. In $LiNiO_2$ only Ni^{3+}/Ni^{4+} is active, while both Ni^{2+}/Ni^{3+} and Ni^{3+}/Ni^{4+} occur in $LiNi_{0.5}Mn_{0.5}O_2$. Hence the average potential for $LiNi_{0.5}Mn_{0.5}O_2$ should be lower than for $LiNiO_2$. Even if one be-

Table I. Comparison of experimental with calculated lattice parameters.

Experimental and calculated lattice parameters Comp	Structure (exp or calc)	Lattice parameters
$LiMnO_2$	*C*2/*m* layered	
	exp.	a = 5.44 Å b = 2.81 Å c = 5.38 Å β = 116°
	calc.	a = 5.58 Å b = 2.83 Å c = 5.49 Å β = 117°
$LiMn_{1/2}Ni_{1/2}O_2$	rhombohedral layered	
	exp.(1)	a = 2.892 Å c = 14.301 Å
	exp.(2)	a = 2.894 Å c = 14.277 Å
	calc.	a = 2.914 Å c = 14.398 Å
$LiNiO_2$	rhombohedral layered	
	exp.(1)	a = 2.885 Å c = 14.197 Å
	exp.(2)	a = 2.894 Å c = 14.226 Å
	calc.	a = 2.943 Å c = 14.287 Å

Table II. Comparison between calculated and measured average discharge potentials for the $LiNi_{0.5}Mn_{0.5}O_2$ and $LiNiO_2$ systems. The last column includes a correction to the computed voltage based on the difference between calculation and experiment for pure $LiNiO_2$. The last two rows of the table show the predicted average potentials in the first and last half of the discharge.

	Calculated		Experimental	Adjusted	
$LiNiO_2$	3.17		3.9 [28]	3.9	
$LiNi_{0.5}Mn_{0.5}O_2$	3.22		3.9 [14]	3.95	
$LiNi_{0.5}Mn_{0.5}O_2$	$0.5 < x_{li} < 1$	$0 < x_{li} < 0.5$		$0.5 < x_{li} < 1$	$0 < x_{li} < 0.5$
	2.94	3.51		3.67	4.24

lieved that Mn participates in the redox process the higher potential is difficult to explain, since the Mn^{3+}/Mn^{4+} couple is below that of Ni^{3+}/Ni^{4+}. These experimental and theoretical results are further evidence that strong interactions exist between the redox couples of metals when they are mixed.[23] In general alloy theory,[24] a measure of the effective Ni-Mn interactions can be obtained by comparing the energy of $LiNi_{0.5}Mn_{0.5}O_2$ to the average energy of $LiNiO_2$ and $LiMnO_2$. If $\Delta \mathbf{E}_{mix} = \mathbf{E}(LiNi_{0.5}Mn_{0.5}O_2) - 1/2[\mathbf{E}(LiNiO_2) + \mathbf{E}(LiMnO_2)]$ is negative, Ni and Mn have an effective attractive interaction and the system will be either randomly mixed or ordered, depending on the strength of the interaction and the preparation temperature. If $\Delta \mathbf{E}_{mix}$ is positive, local phase separation into Mn and Ni rich regions is energetically preferred, though random mixing may be achieved if the synthesis temperature is high enough. From calculating the relevant energy numbers in the above equation we find that for $LiNi_{0.5}Mn_{0.5}O_2$ $\Delta \mathbf{E}_{mix}$ is -216 meV per formula unit, indicating a strong ordering (attractive) tendency between Ni and Mn. Similarly, for the delithiated material $\Delta \mathbf{E}_{mix} = \mathbf{E}(Ni_{0.5}Mn_{0.5}O_2) - 1/2[\mathbf{E}(NiO_2) + \mathbf{E}(MnO_2)]$ is computed to be $+50$ meV, indicating repulsive Ni-Mn interactions. These results give some insight as to why the voltage is higher than may be expected for this system. Ni-Mn interactions go from being attractive in $LiNi_{0.5}Mn_{0.5}O_2$ to being repulsive in $Ni_{0.5}Mn_{0.5}O_2$. Hence, to remove lithium one not only has to supply the binding energy for the Li ion and electron, but also the strong energy increase in the system due to the Mn-Ni bonds becoming unfavorable (as that interaction turns from attractive to repulsive). It can be easily deduced that the effect of changes in the metal-metal interactions upon the average discharge potential is given by

$$\Delta\phi = \Delta \mathbf{E}_{mix}(X_{Li} = 1) - \Delta \mathbf{E}_{mix}(X_{Li} = 0)$$

where ϕ is the equilibrium potential over the range $0 < x_{Li} < 1$. For the $LiNi_{0.5}Mn_{0.5}O_2$ system, this result indicates that the potential is raised by about 266 mV over what would be expected if no Ni-Mn interactions were present (*e.g.*, if Ni^{2+}/Ni^{4+} acted in a pure host, without the presence of Mn). These numbers are derived from calculations on an ordered supercell of Ni and Mn. We have estimated that if the Ni and Mn ions were fully randomized (rather than ordered in the supercell that we used for the calculations) the increase in potential would be slightly less and about 200 mV.

The effect of Li on the Ni-Mn interactions can be easily understood, using what is known about the miscibility of oxides.[25] The effective interaction, for studying phase stability and mixing is not the bare ionic interaction but the energy difference between the average of identical pairs (*i.e.*, Ni-Ni and Mn-Mn) and different pairs (*i.e.*, Ni-Mn). Hence the simplest way to sample this difference is to consider the difference in energy between $LiNi_{0.5}Mn_{0.5}O_2$ (where Ni-Mn bonds are present) and $LiNiO_2$ (with Ni-Ni bonds) and $LiMnO_2$ (with Mn-Mn bonds). In the delithiated state, Ni and Mn have the same $+4$ valence and there is no net electrostatic interaction for exchanging their positions. It can be shown that for such iso-valent ions, the net interaction is due to size effects, and is always repulsive.[26] This agrees with our result of a positive mixing energy in the delithiated state. On the other hand, in the lithiated material the different valence of Ni and Mn leads to a strong effective attractive interaction and hence explains the ordering or mixing tendency.

Our results conclusively indicate that in $LiNi_{0.5}Mn_{0.5}O_2$ (and hence in the related systems $Li[Ni_xLi_{(1/3-2x/3)}Mn_{(2/3-x/3)}]O_2$)[14] Ni is the electrochemically active ion and cycles between Ni^{2+} and Ni^4. The material remains kinetically stable against transformation to spinel because Mn is not present in oxidation states lower than $+4$. We recently showed that the very rapid transformation of layered $LiMnO_2$ to spinel is due to the ease with which Mn^{3+} disproportionates to Mn^{2+} and Mn^{4+}.[27] This allows Mn to rapidly migrate through tetrahedral sites as Mn^{2+}. Mn^{4+}, on the other hand, was shown to have a very high activation barrier for diffusion through the tetrahedral site. Hence, layered oxides with only manganese in the $4+$ oxidation state are expected to be quite stable. In cycling between $LiNi_{0.5}Mn_{0.5}O_2$ and $Ni_{0.5}Mn_{0.5}O_2$ the Ni-Mn arrangement remains fixed due to the lack of any transition metal mobility at room temperature, but the interactions between the ions change considerably. In this system, this change in Ni-Mn interactions causes the voltage to increase for the Ni^{2+}/Ni^4 couple over what it would be in a noninteracting matrix.

The class of materials in which the valence of Ni is $+2$ and Mn is $+4$ seems to possess many desirable features for a cathode material. They also point at new and interesting directions for cathode research. The combination of experimental data on highly doped systems, and our understanding of the role of Mn^{3+} in the problems of many Mn-oxides, clearly indicates that stable layered Mn oxides, containing only Mn^{4+} can be made. In these materials Mn has given up its role as an electrochemically active center and is present only as "filler." Hence, other elements that can take on the $+4$ oxidation state in the layered oxide environment, could be selected on the basis of cost, weight, processability, environmental behavior, etc., as a substitute for Mn.

Acknowledgments

The authors acknowledge the support of the National Science Foundation (MRSEC Program) under contract no. DMR 98-08941. Discussions with Dane Morgan, Elena Arroyo, and Anton Van der Ven were helpful in developing the ideas in this paper. Computing resources from NPACI the National Partnership for Advanced Computing Infrastructure (NSF) are gratefully acknowledged.

The Massachusetts Institute of Technology assisted in meeting the publication costs of this article.

References

1. S. K. Mishra and G. Ceder, *Phys. Rev. B*, **59**, 6120 (1999).
2. F. Capitaine, P. Gravereau, and C. Delmas, *Solid State Ionics*, **89**, 197 (1996).
3. A. R. Armstrong and P. G. Bruce, *Nature (London)*, **381**, 499 (1996).
4. I. J. Davidson, R. S. McMillan, H. Slegr, B. Luan, I. Kargina, J. J. Murray, and I. P. Swainson, *J. Power Sources*, **82**, 406 (1999).
5. B. Ammundsen and J. Paulsen, *Adv. Mater.*, **13**, 943 (2001).
6. Y.-I. Jang, B. Huang, Y.-M. Chiang, and D. R. Sadoway, *Electrochem. Solid-State Lett.*, **1**, 13 (1998).
7. B. Ammundsen, J. Desilvestro, T. Groutso, D. Hassell, J. B. Metson, E. Regan, R. Steiner, and P. J. Pickering, *J. Electrochem. Soc.*, **147**, 4078 (2000).
8. H. Wang, Y.-I. Jang, and Y.-M. Chiang, *Mater. Res. Soc. Symp. Proc.*, **548**, 143 (1999).
9. Y. Shao-Horn, S. A. Hackney, A. R. Armstrong, P. G. Bruce, R. Gitzendanner, C. S.

Johnson, and M. M. Thackeray, *J. Electrochem. Soc.*, **146**, 2404 (1999).
10. Y.-M. Chiang, D. R. Sadoway, Y.-I. Jang, B. Huang, and H. Wang, *Electrochem. Solid-State Lett.*, **2**, 107 (1999).
11. C. Storey, I. Kargina, Y. Grincourt, I. J. Davidson, Y. C. Yoo, and D. Y. Seung, *J. Power Sources*, **97-98**, 541 (2001).
12. E. Rossen, C. D. W. Jones, and J. R. Dahn, *Solid State Ionics*, **57**, 311 (1992).
13. M. E. Spahr, P. Novak, B. Schneyder, O. Haas, and R. Nesper, *J. Electrochem. Soc.*, **145**, 1113 (1998).
14. Z. Lu, D. D. MacNeil, and J. R. Dahn, *Electrochem. Solid-State Lett.*, **4**, A191 (2001).
15. B. Ammundsen, J. M. Paulsen, and I. J. Davidson, Unpublished results (2001).
16. G. Kresse and J. Furthmüller, *Comput. Mater. Sci.*, **6**, 15 (1996).
17. M. K. Aydinol, A. F. Kohan, G. Ceder, K. Cho, and J. Joannopoulos, *Phys. Rev. B*, **56**, 1354 (1997).
18. A. Van der Ven, M. K. Aydinol, G. Ceder, G. Kresse, and J. Hafner, *Phys. Rev. B*, **58**, 2975 (1998).
19. C. Wolverton and A. Zunger, *Phys. Rev. Lett.*, **81**, 660 (1998).
20. A. N. Mansour, X. Q. Yang, X. Sun, J. McBreen, L. Croguennec, and C. Delmas, *J. Electrochem. Soc.*, **147**, 2104 (2000).
21. L. Croguennec, C. Pouillerle, and C. Delmas, *J. Electrochem. Soc.*, **147**, 1314 (2000).
22. C. A. Marianetti, D. Morgan, and G. Ceder, *Phys. Rev. B*, **63**, 1 (2001).
23. G. Ceder, Y.-M. Chiang, D. R. Sadoway, M. K. Aydinol, Y.-I. Jang, and B. Huang, *Nature (London)*, **392**, 694 (1998).
24. D. de Fontaine, in *Solid State Physics*, Vol. 47, H. Ehrenreich, and D. Turnbull, Editors, p. 33, Academic Press, New York (1994).
25. G. Ceder, A. Van der Ven, C. Marianetti, and D. Morgan, *Modell. Simul. Mater. Sci. Eng.*, **8**, 311 (2000).
26. P. D. Tepesch, A. F. Kohan, G. D. Garbulsky, G. Ceder, C. Coley, H. T. Stokes, L. L. Boyer, M. J. Mehl, B. Burton, K. Cho, and J. Joannopoulos, *J. Am. Ceram. Soc.*, **79**, 2033 (1996).
27. J. Reed, A. Van der Ven, and G. Ceder, *Electrochem. Solid-State Lett.*, **4**, A78 (2001).
28. C. Delmas, J. P. Peres, A. Rougier, A. Demourgues, F. Weill, A. Chadwick, M. Broussely, F. Perton, P. Biensan, and P. Willmann, *J. Power Sources*, **68**, 120 (1997).